Design and Process/Measurement for Immersed Element Control in a Reconfigurable Vertically Falling Soap Film

by

John Glowa

SUBMITTED TO THE DEPARTMENT OF MECAHNICAL ENGINEERING IN THE PARTIAL FULFILLMENT OF THE REQUIREMENTS FOR THE DEGREE OF

BACHELOR OF SCIENCE
AT THE
MASSACHUSETTS INSTITUTE OF TECHNOLOGY

JUNE 2007

2007 Massachusetts Institute of Technology. All rights reserved.

Signature of Author: .....
Department of Mechanical Engineering
May 11, 2007

Certified by: .....
Russell L. Tedrake
Professor of Electrical Engineering and Computer Science
Thesis Supervisor

Accepted by: .....
John H. Lienhard V
Professor of Mechanical Engineering
Chairman, Undergraduate Thesis Committee

MASSACHUSETTS INSTITUTE OF TECHNOLOGY
JUN 2 1 2007
LIBRARIES
ARCHIVES

[Page Intentionally Left Blank]

Design and Process/Measurement for Immersed Element Control in a Reconfigurable Vertically Falling Soap Film

by

John Glowa

Submitted to the Department of Mechanical Engineering
on May 11, 2007 in partial fulfillment of the
requirements for the Degree of Bachelor of Science in Engineering
as recommended by the Department of Mechanical Engineering

Abstract: Reinforcement learning has proven successful at harnessing the passive dynamics of underactuated systems to achieve least energy solutions. However, coupled fluid-structural models are too computationally intensive for in-the-loop control in viscous flow regimes. My vertically falling soap film will provide a reconfigurable experimental environment for machine learning controllers. The real-time position and velocity data will be collected with a High Speed Video system, illuminated by a Low Pressure Sodium Lamp. Approximating lines of interference within the soap film to known pressure variations, controllers will shape downstream flow to desired conditions. Though accurate measurement still eludes those without Laser Doppler Velocimetry, order of magnitude Reynolds numbers can be estimated to describe the regime of controller inquiry.

Thesis Supervisor: Russell L. Tedrake
Title Professor, Department of Electrical Engineering and Computer Science

Acknowledgements

This project could not have been completed without the support of the Robot Locomotion Group. You have been a limitless reservoir of information and experience. Russ Tedrake encouraged my progress over the life of the project. John William Roberts was ready to answer any question I could propose, which occurred far too infrequently. Katie Byl, Rick Cory, and Alec Shkolnik have more than two decades of combined experimental robotics experience that frequently intersected with my research. Fumiya Iida and Khashayar Rohanimanesh are models of scholarly inquisition whose dedication to learning I hope to emulate. Though my research leaves many unanswered questions, I hope the RLG can attest to its direction and apply my first steps to something worthy of greater scientific recognition.

Steve Proulx & Ron Wiken are incredible designers that CSAIL is lucky to have. I wish we collaborated more often.

Professor John Brisson of the Mechanical Engineering Department here at MIT should be credited for instilling a sense of wonder for thermo-fluid interactions. His class showed that the complexity of natural interactions still overwhelms the scope of any purposed human design. Professor Brisson first introduced me to problems of arbitrary difficulty, and the assumptions required to sleep at night.

Dr. Jim Bales, director of the Edgerton Center, provided an avenue to combine my scientific and visual arts goals. Strobe Project Laboratory is a crash course in analytical imaging that left me with a novel project of my own design and compelling videos that illustrate the results. Dr. Bales assistance did not end with the class, however. He continued to provide advice on components and techniques, even allowing me to use his equipment to accomplish intermediate goals.

The work of Dr. Jun Zhang of NYU's Courant Institute of Applied Mathematics inspired this investigation. Dr. Zhang readily offered advice and invited the Robot Locomotion Group to visit his laboratory. I pray that any mimicry is viewed as flattery and a desire to follow his deep footprints.

The contributors to this project are many, but I am truly most thankful to my family and friends. My work and my life blend far too often. While falling down the rabbit hole of yet another project, you reminded me that I control how deep I go.

Take a deep breath and dive in.

Table of Contents

Introduction 6
1.1 Background 6
1.1.1 Fluid Modeling 6
1.1.2 Soap Film Experiments 7
1.1.3 Reinforcement Learning/Biomimetics 9
1.2 Evolution of the Project 10
1.2.1 Model Based Online Learning 10
1.2.2 Mk1 Soap Film Construction 11
1.2.3 Current Direction 11
Vertically Falling Soap Film as the Experimental Environment 12
2.1 Flow Path 12
2.2 Fluid Circulation 13
2.3 Nozzle Configuration 14
2.4 Tensioning Mechanism 15
Imaging/Sensing 16
3.1 Photographic Setup 16
3.1.1 Illumination 17
3.1.2 High Speed Video System 18
3.2 Software Imaging 20
3.2.1 XCAP Interfacing 20
3.2.2 Matlab Post-processing 20
Testbed Verification 21
4.1 Cylinder Wake Test 21
4.2 Reynolds Number Estimation 21
Future Work 23
5.1 Filament Actuation 23
5.2 Control System 23
5.3 Transition to LDV/PIV 23
5.4 Final Thoughts 23
References 24

Chapter 1

Introduction

This research intended to apply a subset of machine learning algorithms known as reinforcement learning to the control of an underactuated coupled fluid-structural system. The cross-disciplinary nature of this endeavor implies a significant level of complexity that will become clearer by the end of the introduction.

1.1 Background

1.1.1 Fluid Modeling

Man's mathematical representation of fluid behavior can be split into analytical models and computationally predicted solutions. Some Computational Fluid Dynamics (CFD) tools take certain analytical models to be implicit; however, advances in processing power have allowed many of these assumptions to be removed. When attempting any physical simulation, one must bear in mind the limits of a theoretical model and choose an approach accordingly.

Eulerian analytical models by Bernoulli, Laplace, Navier, & Stokes apply Newton's kinematic theories and the conservation of energy to the goal of tractably solving unknown fluid parameters. The cost of this mathematical simplification is the loss of certain fluid variables. The models created by Bernoulli, Euler, and Laplace rely on the conceit of incompressibility and negligible viscosity. Years later, the Navier-Stokes equations incorporate fluid density and viscosity. Thermodynamic effects, nevertheless, require simultaneous solution of separate energy equations. Finally, time dependent or unsteady forms of these models arise from careful manipulation.

CFD attempts to solve the partial derivatives of the non-linear, time-dependent, full form of the Navier-Stokes equation algebraically with the aid of discretization. Consequently, the operational needs skyrocket. The discretized time step, usually prompted by the time scale of the phenomena of interest, proves to be a modeler's easiest choice. However, spatial gridding or meshing – the infinitesimal discretization of control volumes – creates a new layer of complexity. The accuracy of CFD solutions depends heavily on the fitness of a mesh. In fact, a carelessly constructed mesh can elicit incorrect solutions from a reputable flow solver.

The geometry of the boundary conditions motivates all spatial gridding, but abrupt changes in fluid properties fundamentally depend on the fluid itself. Therefore, mesh designers often iteratively improve the resolution of a subset of the mesh local to complex phenomena. The added detail allows a closer approximation of shock locations or points of separation, and the accompanying fluid parameters. The latest CFD packages embrace flexible grids, some including

the latest incarnation of this concept, adaptive gridding. More explicitly, an adaptive gridding program iteratively adds resolution to surface or volume meshes where flow gradients exceed user-specified values. Alternating between grid modification and solver runs, this method ensures that fluid properties converge globally.

Every improvement in accuracy listed above imparts added complexity and operation time. Thankfully, the subject of CFD trials infrequently requires a complete Navier-Stokes solution with thermodynamic effects. Knowing the right tool for the job is a hallmark of a good engineer; not surprisingly, assumptions can be powerful tools.

As processing time decreases in cost, complex simulations can be performed faster and with more accuracy than ever before. However, the impetus for this research – the behavior of Jun Zhang's one-dimensional flag [16] and a desire to create autonomous flight vehicles with maneuverability far beyond current autopilots – relies upon fluid properties that invalidate the assumptions of theoretically-based simulations. An accurate simulation of these goals must also couple fluid and structural boundary conditions, confining high resolution three-dimensional solutions to those with access to thousands of processors [4]. Benjamin Connell's research successfully simulated the phenomena present in Zhang's work, even extrapolating to three-dimensional flexible foils. However, the significant computational load of his method motivated physical construction of an experimental environment in place of modeling. Concluding, the processing cost of adequately simulating any of the project's goals overwhelms the calculations required by reinforcement learning.

1.1.2 Soap Film Experiments

Flowing soap films offer scientists an attainable physical representation of two-dimensional fluid flow. This experimental approach offers considerable choice of Reynolds numbers and can even contain local shocks. Numerous configurations exist, but the apparatus only requires a fluid source and guide lines bounding the flow from the source. Further design issues will be addressed in Section 3.2. Regrettably, soap film experiments do not completely approximate theoretical two-dimensional solution for numerous reasons.

The most common film visualization technique, interferometry, relies on thickness variations. The distribution of excess volume into these variations threatens the assumption of two-dimensionality. That said, these thickness variations neither affect the orders of magnitude separating the film thickness and flow path width, 10^4 to 10^5, nor occur with Reynolds number greater than unity [12]. Air drag on free surfaces presents another three-dimensional effect that further differentiates film results from ideal Pouiselle flow; however, this coupling can be modeled with Navier-Stokes free boundary condition.

Accurate measurement and repeatability in soap film experiments also pose problems. Laser Doppler Velocimetry (LDV), the most widely accepted method for measuring film velocity, still requires special consideration. To protect the optical sensor of the apparatus, its axis must be kept at an angle to the film plane. This angle causes the three dimensional area of interrogation to include more of the film thickness. Regardless of the sacrifice, the sensor is still not safe from

unexpected reflections from thickness variations. The problem is finally solved by the addition of tracker particles and carefully chosen illumination.

Despite the complexity of determining velocity, other parameters are no easier to measure. In fact, film viscosity will vary as a function of film thickness [11]. Logically, this is due to the composition of the soap film, a stratified fluid. Fluid parameters vary across the thickness of a film, complicating attempts to characterize the flow. In a film, the majority of soap molecules create a surfactant layer on free surfaces. This layer has vastly different chemical and physical properties than the contained fluid sheet and the surrounding air, enabling it to contain the fast moving bulk flow. Therefore, a decrease in film thickness allows for greater interaction between the more viscous surface layers, prompting an increase in film viscosity.

The solution composition determines the average life of the film, as well. Adding glycerin increases the robustness of the film [12] and the bulk viscosity. Air currents or dust can cause a film to break by creating unsustainable gradients across the film thickness. Bringing the bulk viscosity closer to the viscosity of the surfactant layer imparts greater damping capabilities to the flow, implying a more stable film.

Rutgers attributes best results to a solution of 1%-2% liquid dishwashing detergent and 98%-99% distilled water. However, as a learning environment for an actuated element, the robustness of the film to both expected and unexpected perturbations trumps any desire to approximate theory. As a final concern, though seemingly innocuous, soap solutions corrode most metals. Rutgers recommends that the solution only come in contact with anodized aluminum, Teflon, glass, or surgical stainless steel.

Despite a litany of qualifiers, illuminating a soap film with monochromatic light can produce astounding visualizations of turbulence, von Karman streets, or other chaotic phenomena with significant qualitative merit.

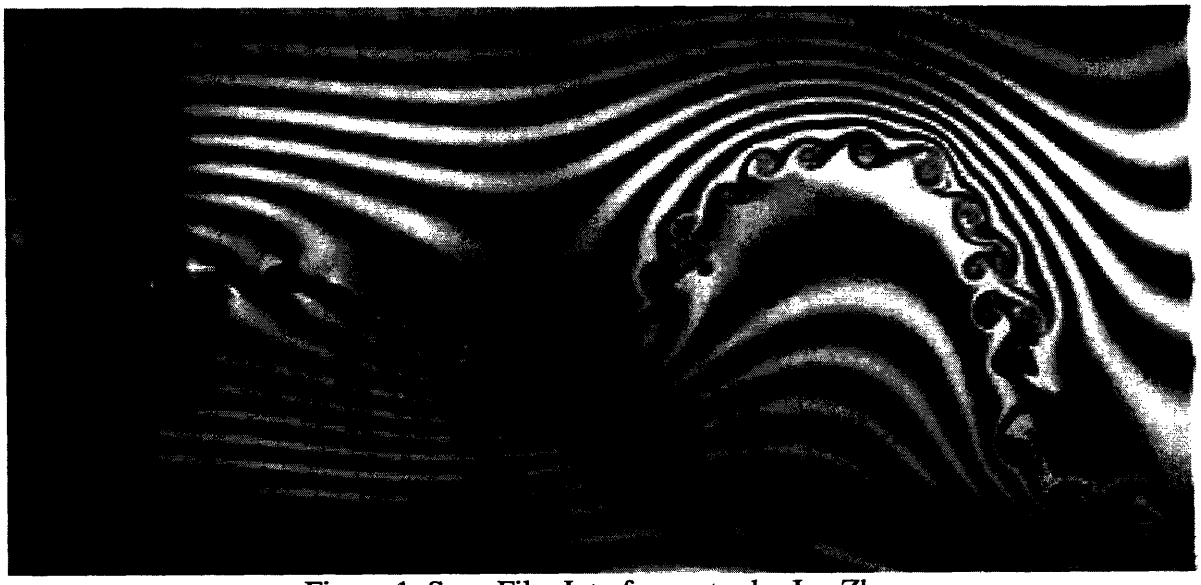

Figure 1: Soap Film Interferometry by Jun Zhang

The alternation of light and dark lines results from a shift of constructive interference to destructive interference. When constructively interfering, the front and rear surfaces of the film reflect back to the camera. The wavelength of light from low pressure sodium bulbs, commonly chosen for film visualizations, closely matches the thickness of the film. Zhang's visualization (Fig. 1) includes both interference lines parallel to the direction of flow and outlining the attached vortex street. These interference lines can therefore be used as a qualitative measure of velocity or pressure gradients.

1.1.3 Reinforcement Learning/ Biomimetics

Fortunately, the difficulty of simulating coupled fluid-structure systems or obtaining practical and accurate fluid parameters from soap film experiments does not prevent the development of an optimal controller. Reinforcement learning, a subset of machine learning, attacks the optimal control problem in a very human way. An actor and critic, even defined as mathematical functions, present an intuitive method for learning. The actor does not need to know his surroundings to begin, but quickly cause and effect relationships will be defined.

More specifically, reinforcement learning balances exploration of new solutions and exploitation of previous successes. Any reinforcement learning algorithm is comprised of a mutable policy (actor), reward, and value (critic) function. The policy function controls the transition from one state to another. The reward function attributes an instantaneous value to a state, while the value function describes one state's connectedness to states with high reward values. The implementation of this approach approximates the learning method present in living organisms.

Around the world, countless birds and fish perform extremely complex energy exchanges between their body structure and a surrounding fluid. Not one of them has the capacity to comprehend the Navier-Stokes equations. Still, they continually outperform all electro-mechanical imposters at finding least energy solutions. This fact alone validates the burgeoning field of biomimetics.

Examples of life's ability to adapt abound. James C. Liao et. al [7] investigated the response of rainbow trout to the von Kármán vortex street emanating from cylinders of different sizes at different flow speeds. The trout adopt a distinctive mode of swimming, dubbed the von Kármán gait, which harnesses energy from the vortices. However, the compelling results of this frequent citation are overshadowed by the fact that man's mechanical mimicry has always far outpaced the capability to mimic intelligence. A credible, adaptable, learning policy is the next hurdle, and many have already taken the first steps.

Augustsson, Wolff, & Nordin [1] applied an evolutionary algorithm to locomotion methods in a rigid wing ornithopter, using four competitors and breeding the winners. Though not by definition reinforcement learning, the fitness function used can be viewed as a value function. Surprising to some, the unique result behaviors could be described as flapping and rowing. This intersection of nature and artificial intelligence will only grow in prevalence as researchers apply machine learning to more complex optimal control problems.

1.2 Evolution of the Project

The choice to adopt a soap film experiment originated from a numerical modeling exercise. The design space for the proposed model is the flow conditions seen in avian flight.

At Reynolds Numbers common to bird flight, $2\text{-}3x10^4$, the steady, inviscid and irrotational assumptions do not hold. Modeling techniques based on these assumptions still operate in this flow regime, and viscosity can be included by means of additional terms. However, the accuracy of inviscid modeling decreases rapidly as $Re < 10^6$.

1.2.1 Model Based Online Learning

Early modeling attempts focused on a vortex sheet approximation for an immersed flexible filament. The vortex sheet approximation functions by replacing boundaries with the mathematical creation of elementary flows. These elementary flows are point sources, sinks, doublets, and vortices. Summing elementary flows with freestream conditions create arbitrary fluid streamlines.

This method was abandoned because of inviscid assumptions, and no simplification in unsteadiness and fluid structural coupling.

1.2.2 Mk1 Soap Film Construction

An early reconfigurable soap film was constructed of plexiglass and repositionable angle brackets. The design is shown below (Fig. 2). The pump chosen for the experiment performed under specifications and the apparatus was abandoned.

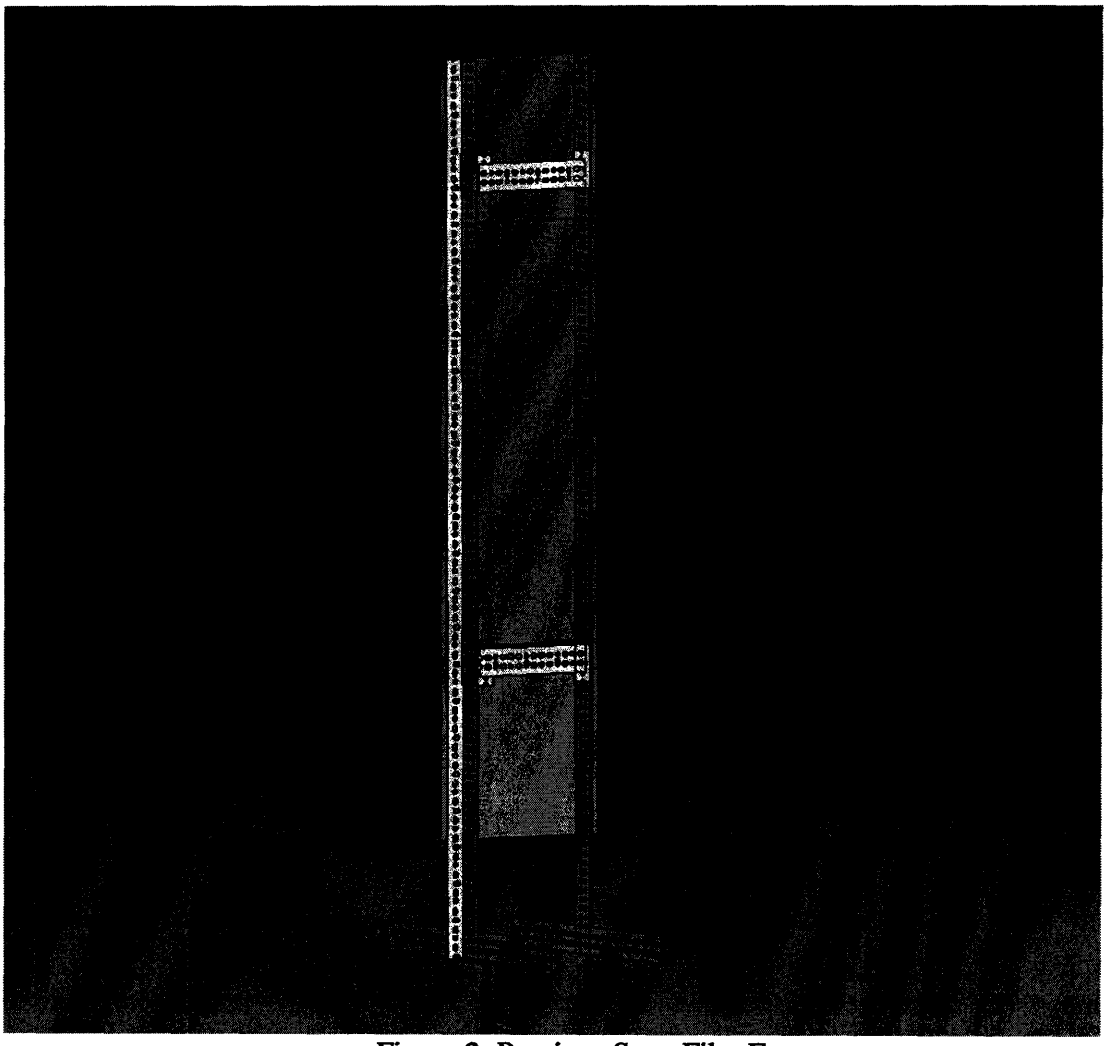

Figure 2: Previous Soap Film Frame

1.2.3 Current Direction

The design motivations evolving from the Mk1 iteration are increased robustness of the structure and perturbation rejection. Secondly, the testbed should accommodate a wide range of modules, creating an open platform for experimentation.

Chapter 2

Vertically Falling Soap Film as the Experimental Environment

The design goals for the experimental environment include: the ability to reconfigure flow channel dimensions, capacity for the greatest range of Reynolds numbers, robustness of the structure, and component simplicity. A gravity-aided, vertical orientation naturally increases the achievable Reynolds numbers, easily furthering a critical goal. Extruded aluminum 80-20© beams comprise the frame (Fig. 3). Machined mounting slots extend along the length of the 80-20©. These slots accommodate any component that can accept two ¼-20 clearance holes, allowing for quick module repositioning. The robustness of the frame is never in question. The dry weight of the mounted components comprises less than 5% of the superstructure's weight; a full reservoir does not significantly alter that percentage. Finally, valve seals fail before structural aluminum surrenders to the effects of corrosion, prompting regular maintenance and inspection.

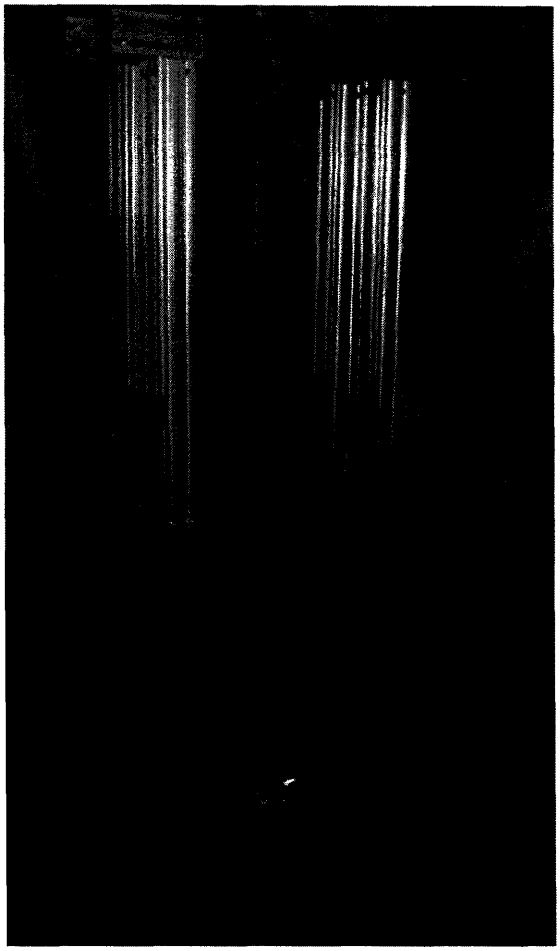

Figure 3: Extruded Aluminum Frame

2.1 Flow Path

The flow path is bounded by two 0.15mm Nylon monofilament lines that meet at the apex and nadir of the channel. Four tensioning lines run perpendicular to the flow direction and define the four corners of the test channel. The most stable fluid parameters occur in a region of constant width after expansion. Consequently, all trials use a rectangular test channel. A small spreading angle, i.e. a larger, more gradual expansion, positively affects the stability of the fluid parameters within the downstream test section. These axioms can be proven theoretically or experimentally.

A careful balance between the injection rate and spreading angle is critical to maintaining a film. Slow flow rates or large spreading angles are not conducive to robust films. The inadequate volume flow thins at the center to meet the guide line boundary conditions. At a critical width, the surfactant layer cannot preserve every boundary condition, and the film bursts. Conversely,

when the injection rate is too great for the spreading angle, a jet of high speed fluid occupies the center of the channel, at times continuing into the test section. The appearance of interference lines in an empty test channel signal unwanted thickness variations, which, in this context, are a result of excess fluid volume. With these basic guidelines, one can quickly develop an intuition for creating robust films

Available structural material limits the height of the entire channel to 1.7m – more than adequate to reach "terminal" velocity. A good nozzle allows for near free fall speed upon injection; however, the spreading of the film quickly increases the surface area undergoing air drag. Rutgers et al. demonstrated in 1996 that velocity in the center of a 5cm wide channel will reach near steady-state after 60cm. After that point, the velocity increases more slowly. This more gradual change coincides with film thinning to maintain constant flux.

The area of focus in the test channel is 70-80cm downstream of injection. At a maximum width of 15cm, the test channel is larger than those found in supporting texts. The widest value is obtained with a 20% glycerin composition. Though greater width and viscosity imply lower velocities, the bulk changes reduce boundary reflections and increase robustness to actuation/vibration. Now, increasing the injection rate produces the desired film speed with lower Reynolds numbers in the transverse directions.

Contraction of the channel is not necessary, but can simplify the re-wetting process. When the nadir is weighted at a single point, releasing the tensioning lines brings the guide lines together. Since the contraction to a single point does not affect upstream properties, the collection angle can be made arbitrarily small. However, the tensioning lines will undergo increased stress as the contraction section shrinks in relation to the expansion section.

2.2 Fluid Circulation

The desired operating point of the soap film is a vertical speed of 250cm/s at a pressure head of 2m. Assuming an 8.5cm width and 3.5um thickness, this translates to a volume flow of ~270ml/hr.

A wide range of self-priming pumps achieve this flow rate and pressure head; therefore, the parameters of maximum flow rate, mechanical simplicity, and cost informed the final decision. A Randolph Econ II Fixed Speed peristaltic pump affordably and simply produces twice the desired flow rate but lacks the flexibility of variable RPMs. This feature doubles the price of many pumps and often proves unwarranted.

Initially hoping to directly connect the output of the pump to an injector, the intercession of better judgment and all related literature encouraged the addition of a pressure head. A peristaltic pump operates by contracting a segment of a hose and advancing the contracted area along the length of the hose repeatedly. Though rhythmic, this behavior is still time dependant. In this case, the pressure head (Fig. 4) functions as a fluid capacitor, damping unsteadiness in the flow. The raised reservoir also allows remixing to combat radial stratification as the fluid travels along the tube towards the injector. A second reservoir at the base of the structure collects fluid for the peristaltic pump to recirculate.

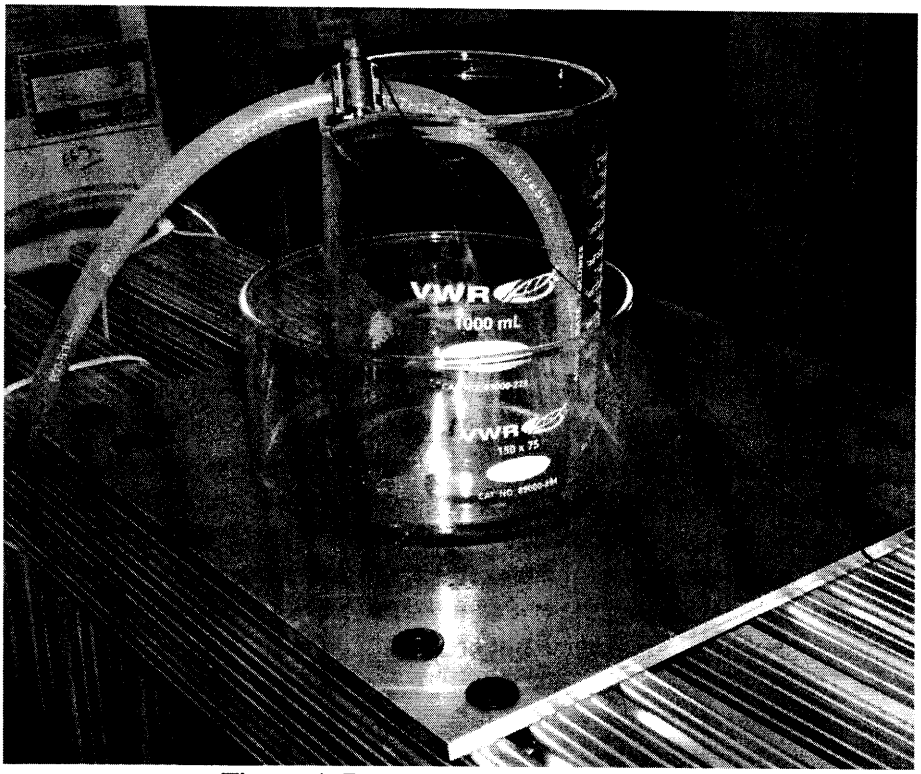

Figure 4: Pressure Head and Spillover

Consultation with Jun Zhang and John William Roberts aided the sizing of the injector pressure head (20-30cm). A 15cm tall 1000ml Pyrex vessel placed within a second Pyrex vessel measuring 7.5cm tall and 750ml assure a constant pressure head. The smaller vessel collects spillover from the larger vessel and directs the fluid back to the ground-level reservoir. Modification of the Pyrex to accommodate a valve and the secondary recirculation path requires sandblasting through the base of both vessels and the side of smaller, respectively.

2.3 Nozzle Configuration

Micropipette tips are an easily modified, nearly disposable nozzle. For example, removing segments from the tip increases the exit diameter. Likewise, plastically deforming the end of the tip creates an elliptical exit, more easily accommodating the guide lines. Finally, replacements are ubiquitous for this common chemical tool.

Two elements of the design – threading the micropipette tip onto the valve, and placing the guide lines in significant tension – prohibit suggested methods of fixing guide lines threading through the nozzle. Tying the guide lines around an inverted segment of a micropipette tip within the main nozzle solves the earlier problems but undoubtedly complicates the flow. Luckily, the uncertainty occurs before the contraction at the exit and settles to a steady-state effect over time. Though the inclusion in the nozzle may produce a constant pressure drop, the contraction and expansion spatially redefine the fluid properties.

2.4 Tensioning Mechanism

The most far-reaching goal for this module is autonomous rewetting upon film bursts. Though exciting, this feature only pays dividends when conducting unsupervised trials for longer than thirty minutes. The soap film experimental environment, still in the process of validation, has not yet supported a reinforcement learning trial. Continual urging to move onto the next roadblock produces a simple but functional, hand-tensioned mechanism.

The four tension lines pass through aluminum bearing surfaces of variable height which determine the test channel dimensions. Each of these lines then attaches to an eyebolt of variable distance below the bearing surface. When the tension lines are disconnected from the eyebolts, the weight at the nadir of the guide lines contracts the channel.

Chapter 3

Imaging/Sensing

The title of this chapter may imply analysis less rigorous than measurement. However, the commonly encountered difficulties of coupled or stratified flow parameters and planar accuracy (1.1.2) call into question the validity and usefulness of any local value. The methods below are more a function of attainable hardware and previous experience, rather than a desire to avoid numbers. Regardless, a High Speed Video system can reveal high frequency and unsteady fluid phenomena in surprising detail.

3.1 Photographic Setup

Scientific photography is a careful interplay of spatial relationships, lighting, and focus, which may fall victim to the lack of perfect solution. Often the phenomena of interest are beyond the capability of publicly available products and necessitate more than one piece of specialized hardware.

Beginning with a simple example, the Lensmaker equation can aid the choice of focal length based upon working distance and the subject size. However, a variation in expected lighting could have far reaching effects on the entire photographic setup. If an underperforming bulb forces an unwarranted increase in aperture, the diminished depth of field may no longer include the subject itself. Though this example only applies to a lens already at its minimum working distance, this fact applies the current photographic setup.

Further underscoring the need for abundant light, HSV exposure times frequently necessitate the minimal path length from light to subject to photoreceptor. Higher sensitivity photoreceptors lessen these concerns but come at a significant cost premium. As the amount of light increases, one must also reduce reflection from elements of the apparatus other than the subject. This is usually accomplished by covering components within the imager's viewing area with matte black photo paper. The water resistance of the matte material prompted investigation; however, experience proved that moisture on the surface does not greatly increase reflection.

The photographic setup that consistently produces the clearest images relies on the largest focal length available and the accompanying low working distance. Iterative reduction of light and photoreceptor distance from the soap film produces a clustering at the superstructure base. The decreased path length in conjunction with an open aperture grants the highest frame rates. The minimum working distance of the 75mm lens establishes a boundary condition for the imager. The figure below (Fig. 5) represents the final arrangement of imaging equipment.

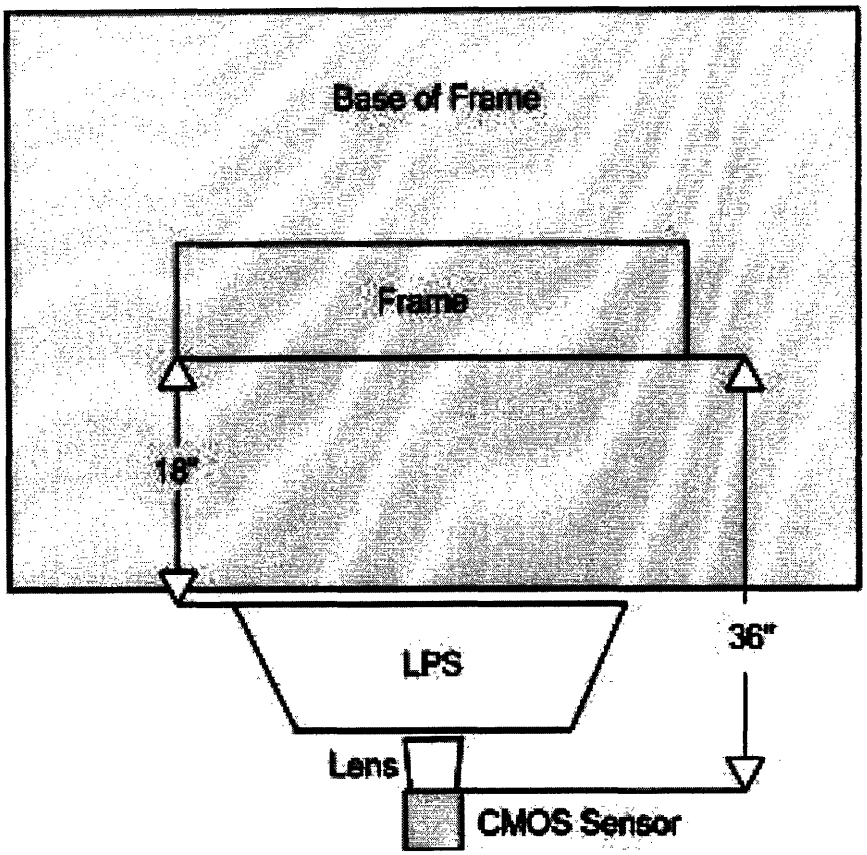

The LPS is angled above vertical. The Lens is angled below vertical. Height and angle are determined by the position of the element.

Exposure: .25ms
Pixel Clock: 74Mhz

Figure 5: Photographic Setup

3.1.1 Illumination

Low Pressure Sodium (LPS) bulbs emit monochromatic light at a frequency of 590nm. Soap film thicknesses can range from two to twenty multiples of the incident wavelength. Consequently, tuning the thickness of the film to the closest integer multiple of 590nm will result in constructive interference.

Furthermore, uncertainty over the film's thickness does not preclude achieving desired visualizations. In this case, varying injection rate until the test channel is clear of dark, destructive interference lines visually accomplishes the goal of instating constructive interference.

One must keep in mind that monochromatic light does not imply frequency independence of the source. Electron discharge, and the resulting current from cathode to anode within a LPS bulb, excites the lone valence electron of sodium vapor enough to discharge a photon of the aforementioned wavelength. The resulting electric potential across the lamp would motivate a migration of sodium ions to a single electrode, if the electrode voltages and accompanying current did not alternate in sign.

A drop in lumen output occurs at a frequency of ~40Hz, proving to be an inseparable effect of alternating current. The only possible solution is the addition of two more LPS lamps, identical

to first, each 40Hz out of phase with the previous. Creating this phase lag is possible with a controlled circuit or a three phase source powering each light with a separate conductor.

Premature integration of two more lamps into a lag circuit would distract from experimental testing. The regular oscillation darkens a number of frames; still, a slightly noisy representation of the fluid is available after post processing.

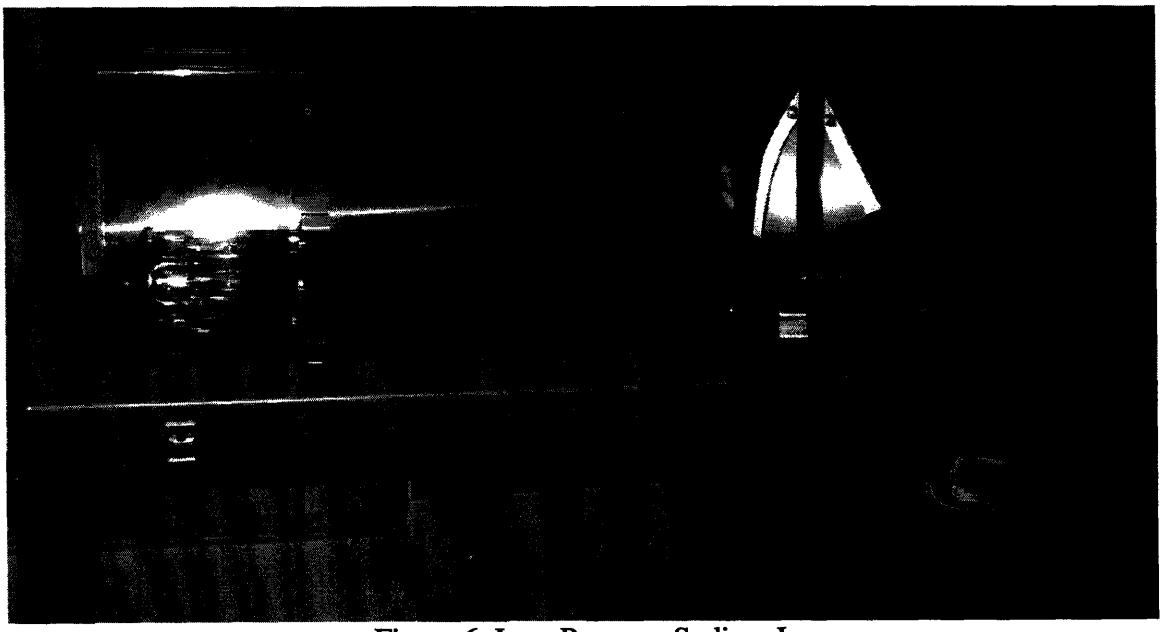

Figure 6: Low Pressure Sodium Lamp

Currently, the experimental environment is lit by a 90W LPS lamp (Fig. 6), nearly a threefold increase of the output from the first imaging trials. Another tripling in power from the phase lagged solution may not be warranted, in fact. Though the path length from bulb to photoreceptor can grow, exposure times are nearly at a minimum. Closing the aperture would only bring more volume around the soap film into focus, not improve overall image quality.

3.1.2 High Speed Video System

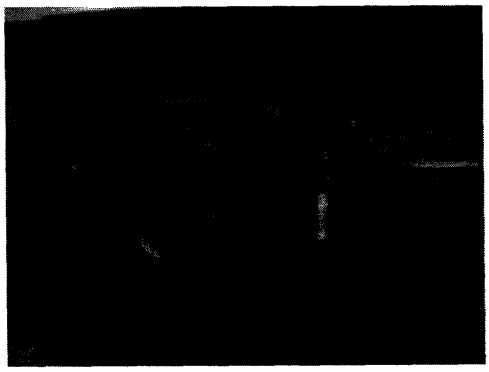

Figure 7: SI-640M

Only recently, a Silicon Imaging SI-640M added a new level of functionality to this multi-disciplinary endeavor. The main data collection tool for the soap film, the SI-640M is a monochromatic bufferless CMOS imager (Fig. 7). The camera connects to an EPIX Inc PIXCI CL1 frame grabber (Fig. 8) through a Cameralink cable with a maximum bandwidth of 8.3Gb/s. This transfer capacity far exceeds the advertised data streams from the imager (96Mb/s) or a burst transferring PCI interface (133-533Mb/s). The CL1 supports registry and driver configuration to increase throughput, though the solutions to these bottlenecks appear in the following section.

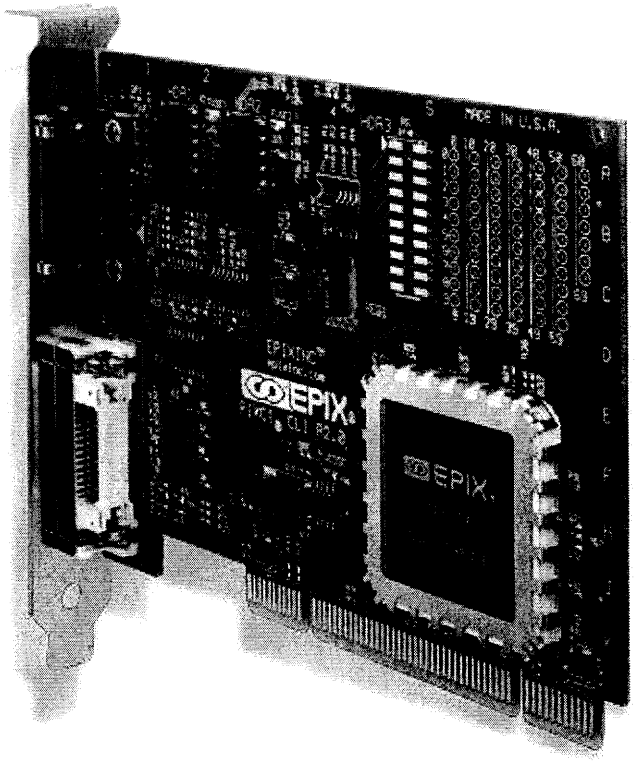

Figure 8: EPIX Inc PIXCI CL1

The highly configurable imager is the most important component of the HSV system. The resolution and frame rate are customizable by multiple methods. The imager supports both reductions of interrogation area and increases in clock speed. In addition, interlaced sub-sampling can be activated at any clock speed or interrogation area. This technique doubles the rate of capture by halving the vertical scan lines in each frame. As a final note, only vertical decrements in area of interrogation (AOI) increase the frame rate. This fact reveals that the scan lines of the CMOS run horizontally and can be sub-sampled odd/even.

3.2 Software Imaging

3.2.1 XCAP Interfacing

Within the included XCAP interface, a user can define such variables as the AOI, pixel clock, exposure time, and multiple gains. After that, a C script is required to grab frames from the imager. The required functions for extracting and saving images from the EPIX board can be found in the XCLIB libraries.

3.2.2 Matlab Post-processing

Once the images have been saved on the hard drive, a matlab script can determine the average brightness of well lit frames. A script can be written to level the brightness across all frames and compile the separate images into a continuous video.

Chapter 4

Testbed Verification

4.1 Cylinder Wake Test

Figure 9: Cylinder Wake at Re ~ 100

The photograph above is the clearest imaging of a vortex street captured with the current equipment. Owing to a terminal velocity that accounts for air drag, the mean velocity, v, can be estimated at 2m/s. Linearly approximating the kinematic viscosity of the mixture from 5.29cSt at a 50% dilution, the dynamic viscosity, ν, of a 20% dilution of glycerin with water will measure 2cSt. This value, $2x10^{-6}$ m^2/s, is near that of water, $1x10^{-6}$ m^2/s. The diameter of the immersed cylinder is .0381mm. Therefore, the Reynolds number of the shedding wake, with $Re = \frac{vD}{\nu}$, is of order 10-100.

4.2 Reynolds Number Estimation

Accurately measuring the mean velocity of the soap film is not trivial. As referenced in the introduction, most published papers determine the velocity of tracker particles illuminated by lasers. The components required are financially prohibitive and merit new solutions.

A soap bubble impinged on the surface of the 2-D film may be approximated as the mean downward velocity if certain forces on the bubble are neglected. Assuming a hemispherical bubble for now, skin friction drag increases with R^2 while pressure drag increases with R. Naturally, an impinged bubble seeks to minimize the effects of drag and decreases its protrusion from the surface.

As friction drag acts along the entire air boundary, the additional area created by a flattened bubble and subsequent resultant force can be neglected. The pressure drag has also been minimized by the flattening, and can be neglected by an order of magnitude argument with respect to the viscous force of the film carrying the bubble along.

However, the effect of the radius of the bubble on the error of this argument is a direction for further exploration.

Chapter 5

Future Work

The scientific merit and usefulness of this project can be increased in many areas. Actuation of immersed members within the flow has been prototyped, but not proven robust or repeatable. The amount of data that can be extracted from the interference lines is still a lingering concern. The Robot Locomotion Group hopes that a well defined policy will overcome any deficiencies in measurement.

5.1 Filament Actuation

John William Roberts is exploring piezo-electric actuation of a flexible fiber or immersed cylinder. Piezo-electrics offer the benefits of small travel and high frequencies of actuation. The length of travel and possible vibration frequencies are on the order of the relevant parameters of the flow path and the transition to unsteadiness studied by Jun Zhang.

5.2 Control System

Most likely, a dynamic policy will vary the forcing frequency of the piezo-electric actuator while a value function weights output with minimal disturbance to mean flow thickness. Further optimization can select policies that generate mean thrust or lift by weighting thickness variations in quadrants surrounding an immersed element.

5.3 Transition to LDV/PIV

The addition of Laser Doppler or Particle Imaging Velocimetry will provide more accuracy to velocity predictions. This will allow the obtained results to be compared to the regimes attained in published papers. However, it is unlikely that the data from more advanced velocimetry techniques can be incorporated into a controller. At Reynolds numbers greater than 10^3, a computer will not be able to resolve the location of tracker particles in real time to provide input to a controller. Addition of a tracker particle mixer is a further logistical hindrance.

5.4 Final Thoughts

When I first began this project, the goals seemed clear and a path was laid out. However, every problem can be viewed with arbitrary complexity. A bump on a flat plate has baffled fluid dynamicists for years. I encourage those that read this paper to choose a project, recognize the depth first, then attempt the breadth.

References

1. Augustsson, Wolff, Nordin. "Creation of a Learning, Flying Robot by Means of Evolution." Proceedings of the Genetic and Evolutionary Computation Conference, GECCO 2002 (pp. 1279-1285). New York, 9-13 July 2002. Morgan Kaufmann.

2. Belmonte, Martin, and Goldburg. "Experimental study of Taylor's hypothesis in a turbulent soap film". arXiv:physics/9905055. v2 1. Jun 1999

3. J. M. Chomaz, and B. Cathalau. "Soap films as two-dimensional classical fluids." *Physical Review A.* 15 February 1990. Vol 41. No. 4.

4. Benjamin Connell. Numerical Investigation of the Flow-Body Interaction of Thin Flexible Foils and Ambient Flow. Ph.D. Thesis, MIT. 2006.

5. R. H. Kraichnan and D. Montgomergy. "Two-dimensional turbulence." *Rep. Prog. Phys.* **43**, 547 1980.

6. Kim, Joongnyon, and Sung, H.J.."Wall Pressure Fluctuations in a Turbulent Boundary Layer over a Bump". AIAA Journal. Vol. 44, No. 7, July 2006

7. Liao, James C. "The Kármán gait: novel body kinematics of rainbow trout swimming in a vortex street." *Journal of Experimental Biology.* 2003. 1059-1073.

8. Mason, Richard. "Fluid Locomotion and Trajectory Planning for Shape-Changing Robots". Doctorate Thesis. California Institute of Technology. 2003.

9. M. Rivera, P. Vorobeiff, and R. Ecke. "Turbulence in Flowing Soap Films: Velocity, Vorticity, and Thickness Fields." *Phys. Rev. Lett.* **81**, 1417 ~1998.

10. M. Rivera and X. Wu. "External Dissipation in Driven Two-Dimensional Turbulence." *Phys. Rev. Lett.* **85**, 976 ~2000.

11. Roushan, Pedran, and Wu, X.L. "Universal Wake Structure of Karman vortex streets in two-dimensional flows". Physics of Fluids. 17, 073601. 2005

12. Rutgers, M.A., Wu X.L., Daniel, W.B. "Conducting fluid dynamic experiments with vertically falling soap films." *Review of Scientific Instruments.* July 2001. 72 (7).

13. Rutgers, M.A., Wu X.L., Bhagavatula, R., Petersen, A.A., Goldburg, W.I., "Two-dimensional velocity profiles and laminar boundary layers in flowing soap films". 1996 American Institute of Physics. S1070-6631(96)00810-0

14. Sutton, Richard S. & Barto, Andrew G. Reinforcement Learning: An Introduction. A Bradford Book. The MIT Press. http://www.cs.ualberta.ca/%7Esutton/book/ebook/the-book.html.

15. Vorobieff & Ecke. "Cylinder wakes in flowing soap films". Physical Review E. Volume 60, Number 3. September 1999.

16. Yu, Junzhi et. al. "Development of a Biomimetic Robotic Fish and its Control Algorithm". IEEE Transactions on Systems, Man, and Cybernetics—PART B: CYBERNETICS, VOL. 34, NO. 4, AUGUST 2004.

17. Zhang, Jun et al. "Flexible filaments in a flowing soap film as a model for one-dimensional flags in a two dimensional wind." *Nature*. 14 December 2000. 408:835-839.

18. Zhu, Luoding and Peskin, Charles S. "Simulation of a Flapping Flexible Filament in a Flowing Soap Film by the Immersed Boundary Method."

This document was created with Win2PDF available at http://www.win2pdf.com.
The unregistered version of Win2PDF is for evaluation or non-commercial use only.
This page will not be added after purchasing Win2PDF.